CDK2 is required for proper homologous pairing, recombination and sex-body formation during male mouse meiosis

Alberto Viera[1], Julio S. Rufas[1], Inés Martínez[2], José L. Barbero[3], Sagrario Ortega[2] and José A. Suja[1,*]

[1]Unidad de Biología Celular, Departamento de Biología, Edificio de Ciencias Biológicas, Facultad de Ciencias, Universidad Autónoma de Madrid, Calle Darwin 2, 28049 Madrid, Spain
[2]Biotechnology Program, Centro Nacional de Investigaciones Oncológicas, Calle Melchor Fernández Almagro 3, 28029 Madrid, Spain
[3]Departamento de Biología Celular y del Desarrollo, Centro de Investigaciones Biológicas, Calle Ramiro de Maeztu 9, 28040 Madrid, Spain
*Author for correspondence (e-mail: jose.suja@uam.es)

Accepted 23 March 2009
Journal of Cell Science 122, 2149-2159 Published by The Company of Biologists 2009
doi:10.1242/jcs.046706

Summary

Cyclin-dependent kinase 2 (CDK2) was assumed to be essential in the mammalian cell cycle both at the G1-S transition and throughout the S phase. Interestingly, ablation of *Cdk2* in mice does not have substantial consequences for embryonic or postnatal development, but both males and females are infertile. In the present study, we have analysed the meiotic alterations leading to infertility in *Cdk2*$^{-/-}$ male mice. We have studied the distribution and dynamics of several proteins related to meiosis progression, such as synaptonemal complex proteins, cohesin complexes, and centromere-, telomere- and recombination-related proteins. *Cdk2*$^{-/-}$ spermatocytes show an incomplete chromosome pairing, an extensive non-homologous synapsis and arrest at a pachytene-like stage with unrepaired programmed double-strand breaks. In these spermatocytes, some telomeres do not attach to the nuclear envelope, and sex chromosomes do not form a sex body. Our data demonstrate an unpredicted participation of CDK2 in the accurate pairing and recombination between homologues during mammalian meiosis.

Supplementary material available online at
http://jcs.biologists.org/cgi/content/full/122/12/2149/DC1

Key words: CDK2, Chromosome synapsis, Meiosis, Meiotic recombination, Mouse, Sex body

Introduction

The progression through the various phases of the cell cycle and subsequent cell divisions in eukaryotic cells is driven by a group of serine/threonine protein kinases, termed cyclin-dependent kinases (CDKs). CDKs are highly conserved from yeast to humans, and their catalytic activity is regulated by their binding to regulatory subunits (named cyclins), whose levels vary during the cell cycle (for a review, see Hochegger et al., 2008). The mammalian genome has 12 loci encoding CDKs, although only five of them, CDK1-CDK4 and CDK6 have been directly implicated in driving the cell cycle (for reviews, see Malumbres and Barbacid, 2005; Santamaria and Ortega, 2006). While CDK1 is generally considered to be a mitotic kinase, the other CDKs are believed to play a role in interphase. The classic model for the mammalian cell cycle includes a sequential participation of CDK4- and CDK6-cyclin D and CDK2-cyclin E complexes in order to prompt cell-cycle entry from quiescence, further progression through the G1 phase, and transition from G1 into S phase in response to mitogenic factors. CDK2-cyclin E complexes and cyclin A (which associates and activates either CDK2 at S phase or CDK1 in G2) have been also related to the progression through the S phase. The final activation of CDK1 by cyclin B ultimately triggers entry into mitosis and subsequent cell division. Nonetheless, compelling information obtained from gene-targeted mouse models for different cyclins and CDKs has demonstrated that, unexpectedly, members of these families show a considerable level of redundancy and that some specific complexes are not required for the mitotic cell cycle. Consequently, there is a need to review and adapt this model (for reviews, see Malumbres, 2005; Santamaria and Ortega, 2006). Thus, although CDK2 has been considered the master key for cell-cycle progression in mammals, both at the G1-S transition (associated to cyclin E) and through the S phase (associated to cyclin A), studies using CDK2 RNAi in cancer cells (Tetsu and McCormick, 2003) and analysis of *Cdk2*$^{-/-}$ knockout mice and mouse embryonic fibroblasts (Berthet et al., 2003; Ortega et al., 2003) have revealed that CDK2 is dispensable for mitotic cell-cycle progression and cell division. Disruption of *Cdk2* in the germ line of mice does not alter either embryonic or postnatal development. However, interestingly, *Cdk2*$^{-/-}$ male and female mice are infertile, with complete penetrance, denoting an unexpected role for CDK2 during gametogenesis (Berthet et al., 2003; Ortega et al., 2003). *Cdk2*$^{-/-}$ male mice show a reduced testis volume, and there is an apparent blocking of meiosis in prophase I that leads to spermatocyte apoptosis and, consequently, to the total absence of mature spermatids (Berthet et al., 2003; Ortega et al., 2003). However, the precise processes that are affected by the lack of CDK2 and that prevent the progression of the meiotic cell cycle beyond early prophase I in spermatocytes are still unknown.

In this study, we have analysed in detail the meiotic progression of spermatocytes in *Cdk2*$^{-/-}$ male mice to better understand the alterations leading to their arrest in prophase I and the putative functions of CDK2 during meiosis. For this purpose, we have analysed the presence, subcellular distribution and cell-cycle-regulated dynamics of some relevant proteins related to meiosis

progression in both squashed and spread *Cdk2*$^{-/-}$ spermatocytes. We have also studied relevant meiotic processes during prophase I, such as formation of the synaptonemal complex and the cohesin axes, specific histone modifications, chromosome pairing and synapsis, positioning of telomeres and centromeres, the initiation and maturation of recombination, and the formation of the sex body. With reference to our results, we propose and discuss the potential implication of CDK2 in critical processes during mammalian meiotic prophase I.

Results

The detailed analysis of meiosis in heterozygous *Cdk2*$^{+/-}$ individuals demonstrated that spermatocytes progressed accurately throughout all the meiotic stages: spermatids were formed and specimens were fertile (Ortega et al., 2003). Consequently, since the meiotic phenotype of *Cdk2*$^{+/-}$ individuals was identical to that of wild-type individuals, we will only show images for *Cdk2*$^{+/-}$ and *Cdk2*$^{-/-}$ spermatocytes in order to avoid redundancy in figures, even though all experiments were carried out simultaneously in wild-type, *Cdk2*$^{+/-}$ and *Cdk2*$^{-/-}$ spermatocytes.

Cdk2$^{-/-}$ spermatocytes display aberrant patterns of synapsis and the absence of sex-body formation

It has been previously reported that CDK2 is essential for the correct progression of meiotic prophase I in male mice. *Cdk2*$^{-/-}$ spermatocytes only reach a pachytene-like stage, but their meiotic defects prevent their passage through the pachytene checkpoint and lead them to apoptosis (Ortega et al., 2003). In order to accurately define the meiotic defects in CDK2 knockout male mice, we first analysed the assembly of the synaptonemal complex (SC). For this purpose, we performed a double-immunolabelling of the proteins SYCP3 and SYCP1, structural components of the axial elements (AEs) and lateral elements (LEs) and of the transverse filaments of the central element (CE) of the SC, respectively. In *Cdk2*$^{-/-}$ early leptotene spermatocytes, SYCP3 appeared as multiple short threads inside nuclei (Fig. 1A). As prophase I progressed, those short threads developed into more continuous linear structures, the AEs, from mid- up to late-leptotene (Fig. 1B). At the onset of zygotene, when synapsis initiates, the SYCP3-labelled AEs started to associate and the CE, as detected by SYCP1, began to assemble (Fig. 1C). In later *Cdk2*$^{-/-}$ zygotene spermatocytes, with progression of synapsis, the stretches of SYCP1 increased in length. However, it became evident that *Cdk2*$^{-/-}$ individuals displayed some synapsis abnormalities because, in all late zygotene nuclei, the presence of single unsynapsed LEs between different synapsed regions (i.e. partner switches) could be easily discerned (Fig. 1D). Moreover, it is worth noting that 20.5% (26 out of 127) of late zygotene nuclei showed completely synapsed ring chromosome structures (Fig. 1D). Interestingly, 88.5% (23 out of 26) of these nuclei showed a single ring structure, whereas only 11.5% (three out of 26) presented two ring structures. We did not observed the presence of more than two rings per spermatocyte. The synaptic deficiencies observed as partner switches in late zygotene were even more evident in more advanced *Cdk2*$^{-/-}$ spermatocytes (Fig. 1E). In these spermatocytes (hereafter called 'pachytene-like' spermatocytes), an abnormal pattern of formation of autosomal SCs was observed (Fig. 1E). Thus, instead of the expected 19 fully assembled and individualised autosomal SCs found in wild-type or *Cdk2*$^{+/-}$ individuals (Fig. 1F), the pachytene-like *Cdk2*$^{-/-}$ spermatocytes displayed a high number of partner switches, and a complete synapsis was not observed in any instance (Fig. 1E). Interestingly, in these pachytene-like *Cdk2*$^{-/-}$ spermatocytes the AEs of the sex chromosomes were not discernible as two distinct SYCP3 structures of different lengths. This contrasts with their normal appearance in wild-type or *Cdk2*$^{+/-}$ individuals, where they appeared associated at the so-called pseudo-autosomal region (PAR) (Fig. 1F). Accordingly, a canonical XY or sex body was not detected after staining with 4′,6-diamidino-2-phenylindole (DAPI) in *Cdk2*$^{-/-}$ pachytene-like squashed spermatocytes (supplementary material Movie 1). In order to determine the position of sex chromosomes within the nucleus, and their possible association, we hybridised *Cdk2*$^{+/-}$ and *Cdk2*$^{-/-}$ spread spermatocytes with specific X and Y painting probes. Sex chromosomes always appeared associated at a sex body in *Cdk2*$^{+/-}$ pachytene spermatocytes (Fig. 1I), but randomly positioned in *Cdk2*$^{-/-}$ pachytene-like spermatocytes (Fig. 1G,H). In this sense, in *Cdk2*$^{-/-}$ pachytene-like spermatocytes, sex chromosomes appeared clearly separated from each other in 71.3% (107 out of 150) spermatocytes (Fig. 1G), and located at the same nuclear domain in only 28.7% (43 out of 150) spermatocytes (Fig. 1H). Nevertheless, in none of the scored *Cdk2*$^{-/-}$ nuclei did sex chromosomes appeared synapsed at the PAR or arranged into a sex body, or form part of the ring chromosomes.

Since the chromosomal passenger inner centromere protein (INCENP) has been previously detected at the CE of the SC from zygotene up to late pachytene (Parra et al., 2003), we performed a double-immunolabelling of INCENP and SYCP3 in *Cdk2*$^{+/-}$ and *Cdk2*$^{-/-}$ spermatocytes in order to elucidate its presence at the CE. Our results showed that, like SYCP1, INCENP appeared at synapsed regions in both *Cdk2*$^{+/-}$ (supplementary material Fig. S1A) and *Cdk2*$^{-/-}$ spermatocytes (Fig. 1J). When SYCP3 ring chromosome structures were observed, INCENP was distributed along the entire ring length (Fig. 1J).

To analyse the proper assembly of the LEs in *Cdk2*$^{-/-}$ spermatocytes, we also studied the distribution of SYCP2, a protein component of the AEs and LEs. Our observations showed that, as in wild-type and *Cdk2*$^{+/-}$ spermatocytes (supplementary material Fig. S1B), SYCP2 colocalised with SYCP3 from leptotene up to the pachytene-like stage on both unsynapsed and synapsed regions (Fig. 1K).

Besides the assembly of AEs/LEs of the SC, we also explored the formation of cohesin axes in *Cdk2*$^{+/-}$ and *Cdk2*$^{-/-}$ spermatocytes by analysing the distribution of the cohesin subunit RAD21, a subunit present in both mitotic and some meiotic cohesin complexes whose distribution during prophase I is similar to that reported for the other cohesin subunits (Parra et al., 2004; Suja and Barbero, 2009). The double-immunolabelling of SYCP3 and RAD21 revealed that, as observed in wild-type and *Cdk2*$^{+/-}$ spermatocytes (supplementary material Fig. S1C), RAD21 cohesin axes colocalised with the SYCP3-labelled AEs/LEs in all the prophase I stages found in *Cdk2*$^{-/-}$ spermatocytes (Fig. 1L). Interestingly, the SYCP3 ring chromosome structures observed in pachytene-like spermatocytes also displayed RAD21 labelling along their entire length (Fig. 1L).

Together, these data indicate that CDK2 is not required for the proper assembly of SCs because AEs/LEs are accurately formed in its absence and some degree of synapsis is achieved. Likewise, CDK2 is dispensable for the loading of RAD21-containing cohesin complexes onto chromosomes. However, CDK2 somehow regulates homologous pairing and synapsis since spermatocytes show an aberrant pattern of synapsis in its absence. Additionally, the presence of CDK2 seems necessary to allow formation of the sex body.

Cdk2$^{-/-}$ spermatocytes arrest prior to mid-pachytene

Taking into account the fact that *Cdk2*$^{-/-}$ spermatocytes did not achieve a complete synapsis, we then looked at whether they were able to reach a pachytene-stage in terms of chromatin conformation. To test this, we analysed the distribution of two histone variants, namely the testis-specific histone H1t and histone H3 trimethylated at lysine 9 (H3K9tri-m), the ATR kinase (ataxia-telangiectasia-mutated and Rad3-related protein) and the tumour suppressor phosphoprotein BRCA1 (breast cancer susceptibility gene 1).

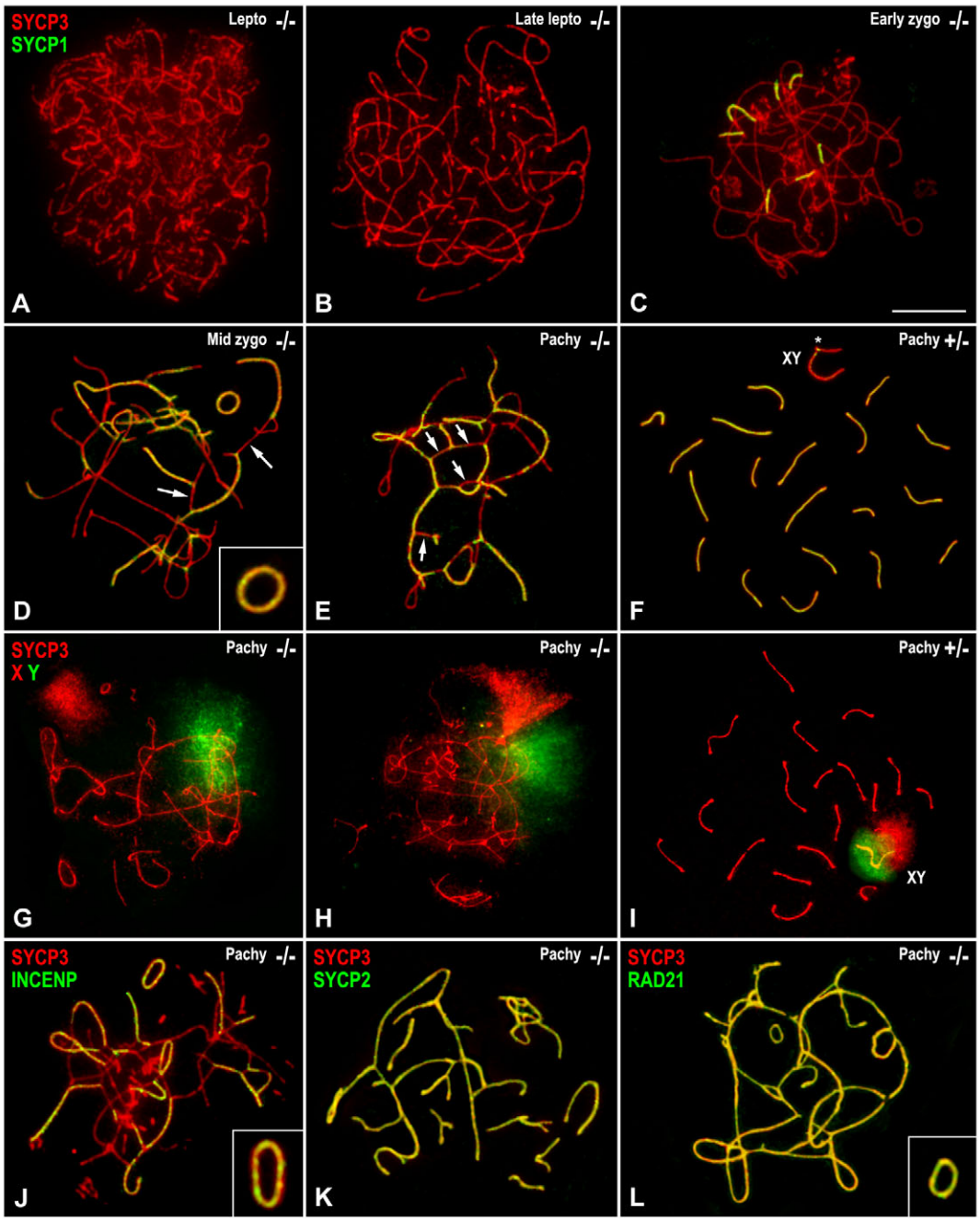

Fig. 1. *Cdk2*$^{-/-}$ spermatocytes show aberrant patterns of synapsis and absence of sex-body formation. Double-immunolabelling of SYCP3 (red in A-F, J-L) with SYCP1 (green in A-F), INCENP (green in J), SYCP2 (green in K) or RAD21 (green in L) in *Cdk2*$^{-/-}$ (A-E, J-L) or *Cdk2*$^{+/-}$ (F) spread spermatocytes. (A-F) Progression of pairing and synapsis in *Cdk2*$^{+/-}$ and *Cdk2*$^{-/-}$ spermatocytes. *Cdk2*$^{-/-}$ spermatocytes show normal loading of SYCP3 on the AEs/LEs during leptotene (A,B) and zygotene (C,D), but a complete synapsis is not visible in the more advanced pachytene-like stages (E). Arrows in D and E indicate the presence of unsynapsed LEs running between different synapsed regions (yellow), i.e. partner switches, in mid-zygotene and pachytene-like spermatocytes. The insert in D highlights the presence of synapsed ring chromosomes. Note the lack of identifiable sex AEs. Pachytene *Cdk2*$^{+/-}$ spermatocytes display normal synapsis (F). The sex bivalent (XY) and the PAR (asterisk) are indicated. (G-I) Immunolabelling of SYCP3 (red) and FISH detection of the X (red) and Y (green) chromosomes in *Cdk2*$^{-/-}$ (G,H) or *Cdk2*$^{+/-}$ (I) spread pachytene spermatocytes. The sex chromosomes may be separated (G) or associated (H) in *Cdk2*$^{-/-}$ pachytene-like spermatocytes, and are always associated at the sex body (XY) in *Cdk2*$^{+/-}$ pachytene spermatocytes. (J-L) INCENP is only detected at the synapsed regions in *Cdk2*$^{-/-}$ pachytene-like spermatocytes. In these spermatocytes SYCP3 colocalises with SYCP2 (K) and the cohesin subunit RAD21 (L) at unsynapsed and synapsed regions. Inserts in J and L correspond to the ring chromosomes observed in the corresponding figures. Scale bar: 10 µm.

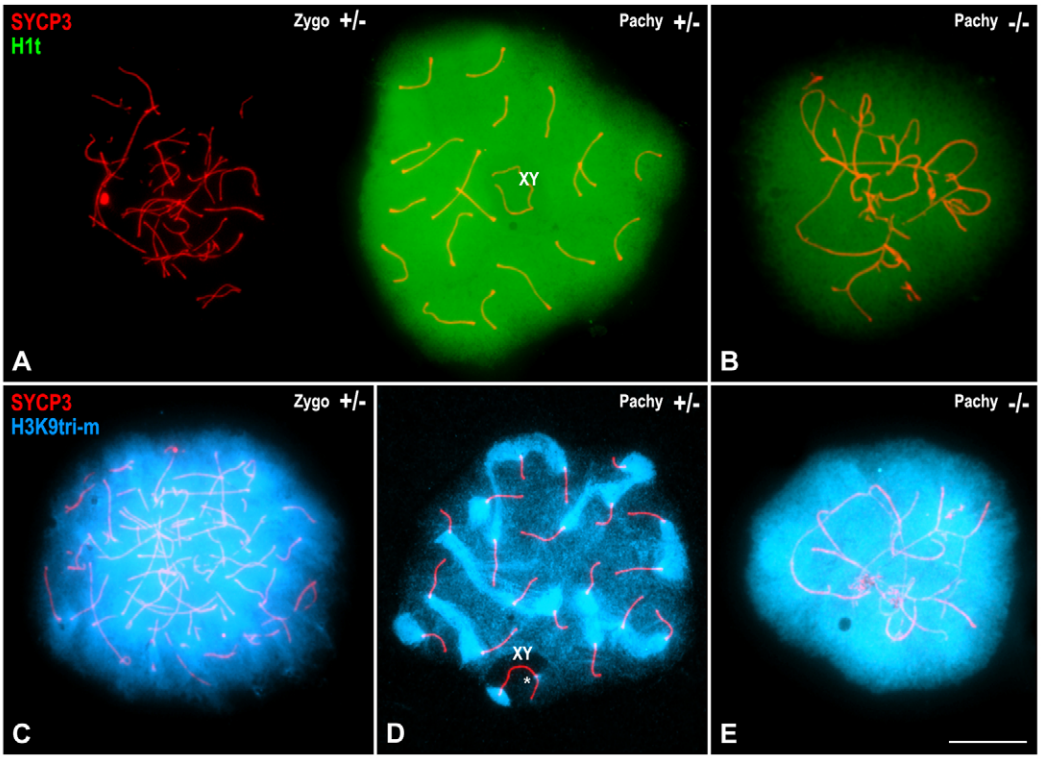

Fig. 2. *Cdk2*$^{-/-}$ spermatocytes arrest prior to mid-pachytene. Double-immunolabelling of SYCP3 (red) with either the histone variant H1t (green in A,B) or H3K9tri-m (blue in C-E) in *Cdk2*$^{+/-}$ (A,C,D) or *Cdk2*$^{-/-}$ (B,E) spread spermatocytes. (A) H1t is not present in zygotene, whereas an intense labelling can be seen in *Cdk2*$^{+/-}$ pachytene spermatocyte. (B) *Cdk2*$^{-/-}$ pachytene-like spermatocytes only display a faint homogeneous H1t labelling over the entire nucleus. (C) In *Cdk2*$^{+/-}$ zygotene spermatocytes, the H3K9tri-m labelling is homogeneously distributed over the nucleus, whereas this labelling is mainly found at centromeric regions in pachytene spermatocytes (D). The sex bivalent (XY) and the PAR (asterisk) are indicated. (E) Pachytene-like *Cdk2*$^{-/-}$ spermatocyte show a uniform H3K9tri-m labelling over the nucleus. Scale bar: 10 μm.

One of the most important molecular markers for determining the entry of spermatocytes in mid-pachytene is the presence of the testis-specific histone H1t (Drabent et al., 1996). As expected, *Cdk2*$^{+/-}$ spermatocytes did not show traces of H1t in zygotene nuclei (Fig. 2A), but presented a massive and intense H1t staining in mid-pachytene nuclei (Fig. 2A). H1t was distributed over the whole pachytene nuclei, even though it seemed to be reduced in the sex body (Fig. 2A). We therefore used the same conditions for observation and imaging capture to analyse and compare the presence of H1t in *Cdk2*$^{-/-}$ spermatocytes. This comparison demonstrated that despite the fact that H1t was also present in *Cdk2*$^{-/-}$ pachytene-like spermatocytes (Fig. 2B), the labelling intensity was always lower than in *Cdk2*$^{+/-}$ mid-pachytene spermatocytes (Fig. 2A,B).

The trimethylation of histone H3 at lysine 9 represents an epigenetic signal, recognised by the heterochromatin binding protein 1 (HP1), which appears to be crucial for the heterochromatin configuration (Lachner et al., 2001). In male mouse meiosis, this methylation process has been related to the correct centromere clustering at the onset of meiosis (Peters et al., 2001). In *Cdk2*$^{+/-}$ spermatocytes, a strong H3K9tri-m labelling was observed throughout the chromatin during leptotene and zygotene stages (Fig. 2C). As described in wild-type individuals (Peters et al., 2001), the H3K9tri-m labelled regions extended beyond the heterochromatic domains (Fig. 2C). By mid-pachytene, H3K9tri-m was preferentially associated to the centromeric heterochromatic regions of the chromosomes and/or bivalents clustered at chromocentres, although some labelling persisted over the entire nucleus (Fig. 2D). By contrast, whereas H3K9tri-m presented a normal distribution pattern (data not shown) in *Cdk2*$^{-/-}$ leptotene and zygotene spermatocytes, in pachytene-like spermatocytes H3K9tri-m remained positioned over the entire nuclei instead of relocating to the centromere regions (Fig. 2E).

BRCA1 and ATR appear as foci along unsynapsed AE/LEs during leptotene and zygotene, even though some foci can also be detectable at synapsed regions during zygotene (Keegan et al., 1996; Scully et al., 1997). In pachytene, both proteins are restricted to the asynapsed portions of sex chromosomes (Keegan et al., 1996; Scully et al., 1997). It has been proposed that BRCA1 recruits the kinase ATR to asynapsed sex AEs and sex chromatin during late prophase I stages (Turner et al., 2004). Consequently, analysis of the distribution and dynamics of ATR and BRCA1 on spermatocytes can be a useful tool for determining the progression through prophase I. Our observations revealed that ATR appeared as foci along the AEs/LEs during leptotene and zygotene in *Cdk2*$^{+/-}$ spermatocytes (data not shown). The number of ATR foci decreased until mid-pachytene when they appeared to be restricted to the asynapsed sex chromosome AEs (Fig. 3A). Additionally, a faint cloudy ATR labelling was observed over the chromatin of sex chromosomes (Fig. 3A). By contrast, leptotene and zygotene *Cdk2*$^{-/-}$ spermatocytes ATR showed the expected pattern of foci distribution (data not shown), whereas pachytene-like spermatocytes showed the persistence of ATR over both synapsed and unsynapsed LEs (Fig. 3B). BRCA1, however, labelled the asynapsed sex chromosome AEs in pachytene *Cdk2*$^{+/-}$ spermatocytes (Fig. 3C), but was not detected in pachytene-like *Cdk2*$^{-/-}$ spermatocytes (Fig.

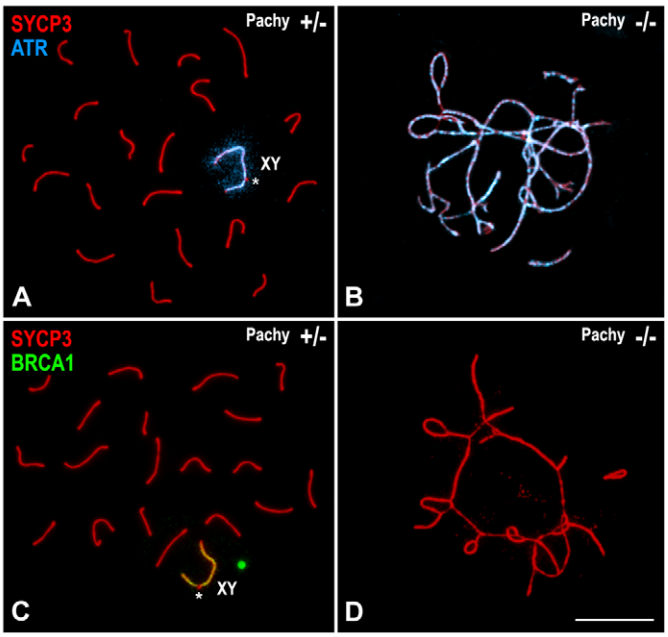

Fig. 3. *Cdk2*$^{-/-}$ spermatocytes arrest prior to mid-pachytene. Double-immunolabelling of SYCP3 (red) with either ATR (blue in A,B) or BRCA1 (green in C,D) in *Cdk2*$^{+/-}$ (A,C) or *Cdk2*$^{-/-}$ (B,D) spread pachytene spermatocytes. (A) In *Cdk2*$^{+/-}$ spermatocytes, ATR labelling is reduced to the asynapsed sex chromosome AEs, and to a faint cloudy signal over the sex body (XY). The position of the PAR is indicated by an asterisk. (B) In *Cdk2*$^{-/-}$ pachytene-like spermatocytes, ATR labels both the synapsed and unsynapsed regions. (C) In *Cdk2*$^{+/-}$ spermatocytes, BRCA1 concentrates along the asynapsed AEs of sex chromosomes and is absent from the synapsed PAR (asterisk). (D) No BRCA1 traces can be observed in *Cdk2*$^{-/-}$ spermatocytes. Scale bar: 10 µm.

3D). Together, these data indicate that *Cdk2*$^{-/-}$ spermatocytes progress through prophase I but arrest prior to mid-pachytene.

Cdk2$^{-/-}$ spermatocytes display non-homologous synapsis

Since *Cdk2*$^{-/-}$ pachytene-like spermatocytes showed frequent partner switches of LEs, we then looked at whether the synapsed regions also corresponded to non-homologous synapsis. For this purpose we first performed a double-immunolabelling of SYCP3 with an anti-centromere serum (Fig. 4A,B). As expected, since mouse chromosomes are strictly telocentric, in wild-type and *Cdk2*$^{+/-}$ pachytene spermatocytes, centromeres were observed as pairs of closely associated broad signals positioned at one of the SC ends of all autosomal bivalents, and at the end of the asynapsed AEs in both sex chromosomes (Fig. 4A). By contrast, the number and position of the centromere signals varied in *Cdk2*$^{-/-}$ pachytene-like spermatocytes (Fig. 4B). Thus, some single centromeres appeared at the end of some unsynapsed LEs, but other centromeres were surprisingly present along fully synapsed regions (Fig. 4B). This observation indicates an important degree of non-homologous synapsis in *Cdk2*$^{-/-}$ spermatocytes. When the SYCP3 ring structures were analysed, two closely associated centromere signals were observed along the SC (Fig. 4B).

We also determined the number and position of telomeres in *Cdk2*$^{-/-}$ pachytene-like spermatocytes by double-immunolabelling of SYCP3 and the telomeric protein TRF1 (Fig. 5). In *Cdk2*$^{+/-}$ spread pachytene spermatocytes, as in the wild type (Scherthan et al., 2000), we always detected 41 telomeric signals: two signals at the ends of each of the 19 autosomal bivalentes and three additional signals on the sex bivalent, one at the proximal end of each sex chromosome, and one at the PAR where their distal ends are associated (Fig. 5A). In *Cdk2*$^{-/-}$ spread pachytene-like spermatocytes (n=21) the number of telomere signals ranged between 25 and 38. Some of these signals were observed at the ends of either unsynapsed or synapsed LEs, whereas many others were unexpectedly observed scattered along the trajectories of the LEs at synapsed regions (Fig. 5B). As with centromeres, groups of TRF1 signals appeared frequently clustered and were included in non-homologous synaptic regions, where chromosomes end-to-end fusions cannot be discarded (Fig. 5B). Additionally, two closely associated TRF1 signals were always observed at the SYCP3 ring structures (Fig. 5B).

To further investigate the disorder observed in the distribution of telomeres in *Cdk2*$^{-/-}$ pachytene-like spermatocytes, we subsequently performed a double-immunolocalisation of SYCP3 and TRF1 on squashed spermatocytes (Fig. 5C-H). Since the squashing procedure preserves the structure and volume of spermatocyte nuclei (Parra et al., 2002), we could accurately analyse the distribution of telomeres in *Cdk2*$^{+/-}$ and *Cdk2*$^{-/-}$ spermatocytes. Our observations demonstrated that in *Cdk2*$^{+/-}$ pachytene nuclei, as in wild-type nuclei (Viera et al., 2003), all 41 telomeric signals were located at the ends of the SCs close to the nuclear envelope (NE) (Fig. 5C-E; supplementary material Fig. S2A, Movie 2). By contrast, the scored number of telomere signals in *Cdk2*$^{-/-}$ pachytene-like squashed spermatocytes (n=10) ranged between 23 and 30. Interestingly, we found that all *Cdk2*$^{-/-}$ squashed pachytene-like spermatocytes showed 11-16 telomere signals not associated to the NE but lying at the nuclear interior (Fig. 5F-H; supplementary material Fig. S2B, Movie 2). We did not observed ring structures associated with the NE in any

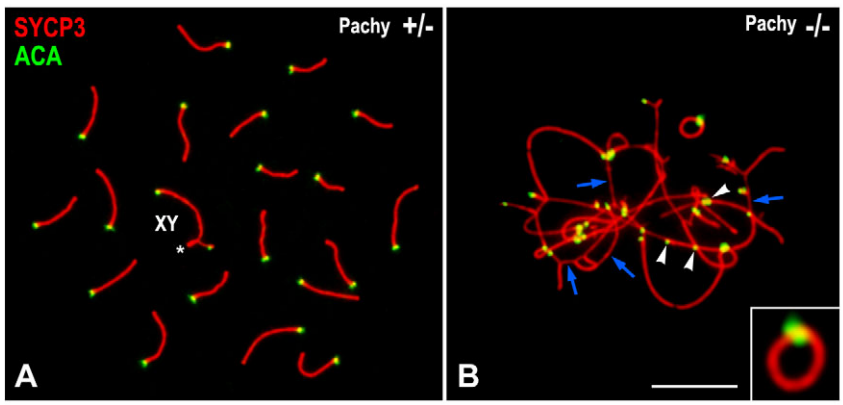

Fig. 4. *Cdk2*$^{-/-}$ spermatocytes display non-homologous synapsis. Double-immunolabelling of SYCP3 (red) and centromeres with an anti-centromere autoantibody (ACA) (green) in *Cdk2*$^{+/-}$ (A) and *Cdk2*$^{-/-}$ (B) spread pachytene spermatocytes. (A) In *Cdk2*$^{+/-}$ spermatocytes, the centromeres are located at one end of each autosomal SC and close to the ends of the asynapsed AEs of sex chromosomes (XY). The PAR (asterisk) is indicated. (B) In *Cdk2*$^{-/-}$ pachytene-like spermatocytes, some centromeres (arrowheads) appear along synapsed regions. Unsynapsed LEs (blue arrows) between different synapsed regions denote non-homologous synapsis. Ring chromosome structures (inset) show two closely associated centromeres. Scale bar: 10 µm.

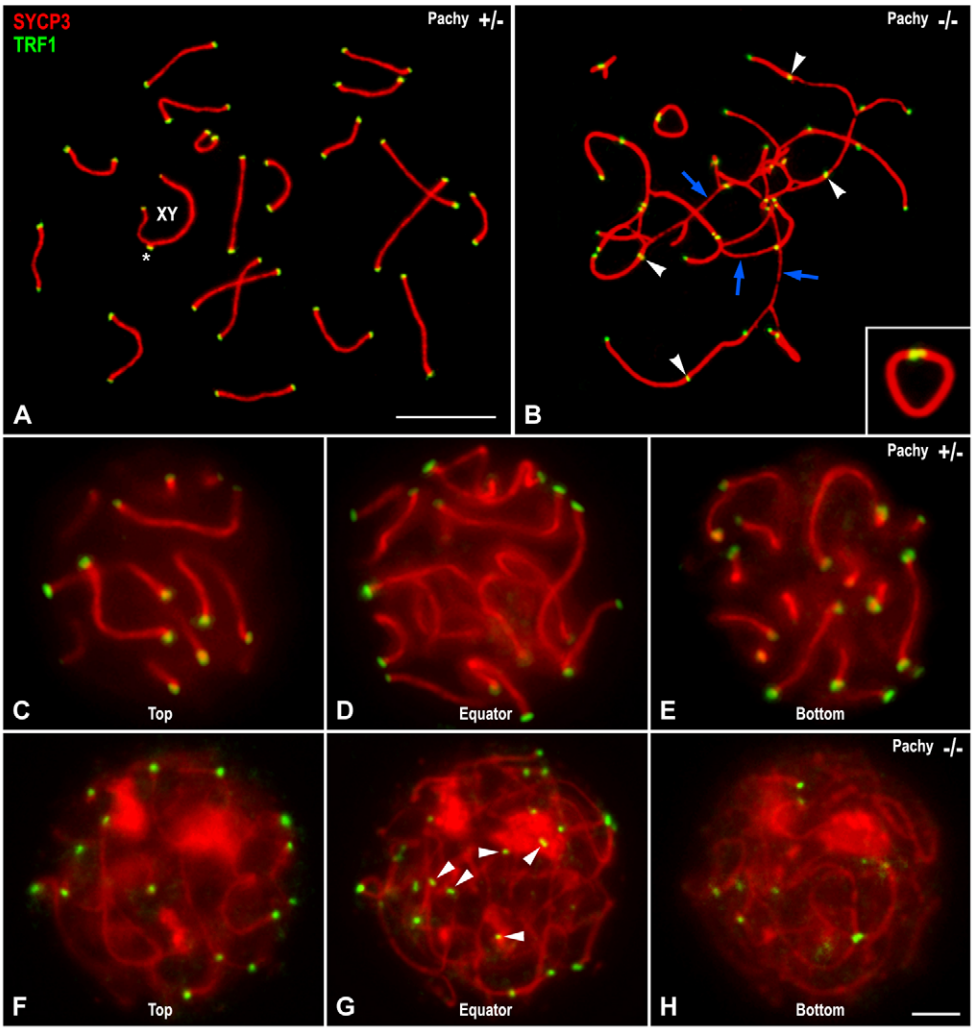

Fig. 5. Telomeres in *Cdk2*$^{-/-}$ spermatocytes are not attached to the NE. Double-immunolabelling of SYCP3 (red) and TRF1 (green) on spread (A,B) or squashed (C-H) *Cdk2*$^{+/-}$ (A,C-E) and *Cdk2*$^{-/-}$ (B,F-H) pachytene spermatocytes. (C-H) Partial Z projections of the top (C,F), equator (D,G) and bottom (E,H) nuclear portions of two spermatocytes. All the projections result from the superimposition of 15 focal planes throughout a certain region. (A) In *Cdk2*$^{+/-}$ spermatocytes, telomeric TRF1 signals appear as spots at both ends of each autosomal SC and at the ends of sex chromosome AEs. The sex bivalent (XY) and the PAR (asterisk) are indicated. (B) In *Cdk2*$^{-/-}$ pachytene-like spermatocytes, some TRF1 signals (arrowheads) are detected along synapsed regions. Some unsynapsed LEs (blue arrows) run between different synapsed regions. (C,E) In *Cdk2*$^{+/-}$ pachytene spermatocytes, telomeres locate at the LE ends that associate with the NE. Thus, TRF1 signals appear in the central region of the images in the reconstructions of the top (C) and bottom (E) regions, and at the nuclear periphery in the equator region (D). (F-H) In *Cdk2*$^{-/-}$ pachytene-like spermatocytes, some telomere complexes are located at the nuclear interior (arrowheads in G). Large accumulations of SYCP3 are detected inside the nucleus. Scale bars: (A,B) 10 μm; (C-H) 5 μm.

instance. Together, our results strongly indicate that some telomeres may fuse in the absence of CDK2, and that about 50% of them do not attach to the NE.

Cdk2$^{-/-}$ spermatocytes accumulate non-repaired double-strand breaks

In mammals, meiotic homologous recombination is initiated at leptotene by the formation of double-strand breaks (DSBs) by SPO11. Immediately after, the histone variant H2AX is phosphorylated at serine 139 (γ-H2AX). This γ-H2AX is detected along the chromatin surrounding the meiotic DSBs (Mahadevaiah et al., 2001). Afterwards, the meiotic recombination machinery is involved in the processing and repair of the DSBs in order to both promote synapsis and generate homologous recombination. This machinery includes, among others, the recombination proteins RAD51, RPA and MLH1 (for a review, see Moens et al., 2007). Since we were interested in underscoring a possible relationship between the synaptic defects observed in *Cdk2*$^{-/-}$ spermatocytes and failures in the recombination pathways, we analysed the distribution patterns of γ-H2AX, RAD51, RPA and MLH1 in *Cdk2*$^{+/-}$ and *Cdk2*$^{-/-}$ spermatocytes.

The formation of DSBs was monitored by the presence of γ-H2AX from the leptotene-zygotene transition in *Cdk2*$^{+/-}$ and *Cdk2*$^{-/-}$ spermatocytes (data not shown). At zygotene, in both *Cdk2*$^{+/-}$ and *Cdk2*$^{-/-}$ spermatocytes, γ-H2AX labelled most of the chromatin at both unsynapsed and synapsed chromosomal regions (Fig. 6A,B). Concomitantly with synapsis progression, γ-H2AX started to fade away and remained confined to the sex body by mid-pachytene in wild-type and *Cdk2*$^{+/-}$ spermatocytes, as previously reported (Fernández-Capetillo et al., 2003) (Fig. 6C; supplementary material Movie 3). Conversely, in pachytene-like spermatocytes lacking CDK2, the γ-H2AX labelling persisted as flare-shaped chromosomal domains protruding from both unsynapsed and synapsed LEs (Fig. 6D; supplementary material Movie 3). This result reveals the accumulation of non-repaired DSBs in pachytene-like *Cdk2*$^{-/-}$ spermatocytes.

We then analysed the distribution of the recombinase RAD51 in *Cdk2*$^{+/-}$ and *Cdk2*$^{-/-}$ spermatocytes. RAD51 is involved in the homology search by loading onto a resected single-strand end flanking a DSB (Hunter and Kleckner, 2001), and is found at the so-called early nodules along leptotene and zygotene AEs/LEs (Moens et al., 2007). The average number of RAD51 foci along AEs/LEs in wild-type (210, n=10), *Cdk2*$^{+/-}$ (215, n=10) and *Cdk2*$^{-/-}$ (222, n=10) zygotene spermatocytes was similar (Fig. 6E,F). During the processing of DSBs, the number of RAD51 foci decreased in both *Cdk2*$^{+/-}$ and wild-type spermatocytes so that by early pachytene an average number of 50 RAD51 foci (n=10 in both cases) remained associated to the LEs of synapsed homologous chromosomes and over the asynapsed AEs of the sex chromosomes (Fig. 6G;

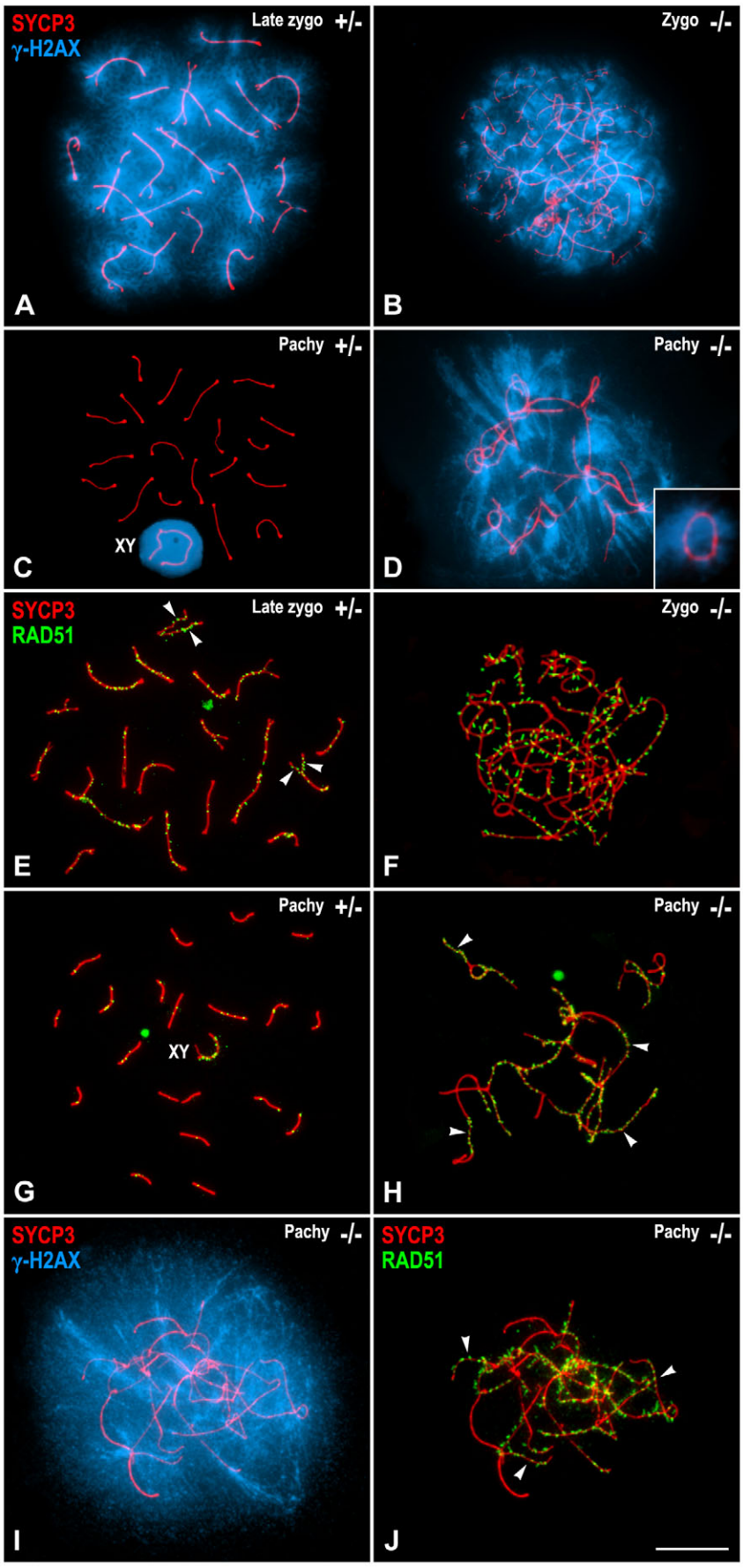

supplementary material Movie 4). The progression of the DSBs repair led to the complete disappearance of RAD51 foci by mid- to late-pachytene in *Cdk2*$^{+/-}$ and wild-type spermatocytes (data not shown) (Moens et al., 2002). By striking contrast, numerous RAD51 foci (average number 224; n=10) were observed along the LEs of *Cdk2*$^{-/-}$ pachytene-like spermatocytes (Fig. 6H; supplementary material Movie 4). It is worth noting that the number of RAD51 foci was higher along unsynapsed LEs (Fig. 6H). A triple-immunolabelling with SYCP3, γ-H2AX and RAD51 revealed that there was no apparent relationship between the massive γ-H2AX labelling and the differential distribution of RAD51 foci in *Cdk2*$^{-/-}$ pachytene-like spermatocytes (Fig. 6I,J). While γ-H2AX labelling was detected over the entire nucleus at both synapsed and unsynapsed regions (Fig. 6I), RAD51 preferentially located at unsynapsed LEs (Fig. 6J). Moreover, no direct relationship could be determined between the bases of the γ-H2AX flare-shaped chromosomal domains, located close to the LEs, and the position of the RAD51 foci (Fig. 6I,J).

Next, we determined the distribution of RPA in *Cdk2*$^{+/-}$ and *Cdk2*$^{-/-}$ spermatocytes. RPA is a single-stranded DNA-binding protein that interacts with RAD51 during the strand-exchange reaction (Sigurdsson et al., 2001) necessary for meiotic recombination (for a review, see Svetlanov and Cohen, 2004). RPA foci appear soon after RAD51 at the so-called transition nodules along zygotene AEs and LEs (Moens et al., 2007). We observed a large number of RPA foci along AEs in both *Cdk2*$^{+/-}$ and *Cdk2*$^{-/-}$ zygotene spermatocytes (not shown). In *Cdk2*$^{+/-}$ pachytene spermatocytes, RPA foci were still visible over the synapsed autosomal LEs (Fig. 7A). Additionally, a large accumulation of RPA was detected at the PAR of the sex chromosomes, and a few RPA foci detected along

Fig. 6. *Cdk2*$^{-/-}$ spermatocytes accumulate non-repaired DSBs. Double-immunolabelling of SYCP3 (red) with either γ-H2AX (blue in A-D,I) or RAD51 (green in E-H,J) in *Cdk2*$^{+/-}$ (A,C,E,G) and *Cdk2*$^{-/-}$ (B,D,F,H-J) spread spermatocytes. (A,B) Massive γ-H2AX labelling is observed over the nuclei in both *Cdk2*$^{+/-}$ and *Cdk2*$^{-/-}$ zygotene spermatocytes. (C) By mid-pachytene, the γ-H2AX distribution is restricted to the sex body (XY) in *Cdk2*$^{+/-}$ spermatocytes, whereas *Cdk2*$^{-/-}$ pachytene-like spermatocytes display intensive γ-H2AX labelling over both synapsed and unsynapsed regions and ring chromosomes (inset) (D). (E,F) Multiple RAD51 foci distribute along the trajectories of unsynapsed (arrowheads in E) and synapsed LEs in *Cdk2*$^{+/-}$ and *Cdk2*$^{-/-}$ zygotene spermatocytes. (G) In *Cdk2*$^{+/-}$ pachytene spermatocytes, the number of RAD51 foci is considerably reduced despite the fact that few foci are still visible in either the autosomal and sex bivalents (XY). (H) In *Cdk2*$^{-/-}$ pachytene-like spermatocytes, a high number of RAD51 foci are mainly located at unsynapsed LEs (arrowheads). (I,J) Triple-immunolabelling of SYCP3, γ-H2AX and RAD51 in a *Cdk2*$^{-/-}$ pachytene-like spermatocyte. No direct correspondence is found between the relative distributions of γ-H2AX and RAD51 and their presence at synapsed or unsynapsed (arrowheads) regions. Scale bar: 10 μm.

their asynapsed AEs (Fig. 7A). In *Cdk2*$^{-/-}$ pachytene-like spermatocytes, and in contrast to what was found for RAD51, RPA foci were mainly detected along synapsed regions (Fig. 7B). Likewise, a large number of RPA foci were observed along the SYCP3 ring structures (Fig. 7B).

Finally, we monitored the expression of MLH1 in *Cdk2*$^{+/-}$ and *Cdk2*$^{-/-}$ spermatocytes. MLH1 is a DNA mismatch repair protein that appears at the so-called recombination nodules along middle- and late-pachytene SCs (Moens et al., 2007); it is the hallmark of reciprocal crossovers and critical for chiasma formation (Baker et al., 1996). In *Cdk2*$^{+/-}$ pachytene spermatocytes, as in the wild type, one or two MLH1 foci were present along autosomal SCs, and one focus at the PAR in the sex bivalent (Fig. 7C). By contrast, no MLH1 foci were detected in *Cdk2*$^{-/-}$ pachytene-like spermatocytes (Fig. 7D). These findings strongly indicate that *Cdk2*$^{-/-}$ spermatocytes initiate meiotic recombination but accumulate non-repaired DSBs.

Discussion

Cdk2$^{-/-}$ spermatocytes undergo an arrest of prophase I that is consistent with their incapacity to progress through the pachytene checkpoint, as previously reported (Ortega et al., 2003). In the present paper we have analysed in detail the meiotic phenotype of *Cdk2*$^{-/-}$ males in order to underscore the meiotic failures that finally result in the massive death of prophase I spermatocytes and, consequently, in male sterility.

CDK2 is required for homologous pairing

In mutant *Cdk2*$^{-/-}$ male mice, meiosis develops accurately during the initial stages of prophase I. This is demonstrated by correct assembly of AEs/LEs along the chromosomes during leptotene and zygotene, as monitored by the proper loading of the AE/LE proteins SYCP3 and SYCP2. Loading of the cohesin subunit RAD21 onto cohesin axes, subjacent to formation of AEs/LEs, also supports their accurate assembly. Likewise, assembly of the SC central element, as monitored by association of the transverse filament protein SYCP1 and the chromosomal passenger protein INCENP (Parra et al., 2003), also takes place in the absence of CDK2 during zygotene. Consequently, CDK2 is not required for the assembly of AEs/LEs and RAD21 cohesin axes during SC formation. However, *Cdk2*$^{-/-}$ spermatocytes did not show complete formation of the tripartite SCs along the entire length of the homologous chromosomes typical of the pachytene stage. Data indicated that the most advanced *Cdk2*$^{-/-}$ prophase I spermatocytes arrested prior to mid-pachytene and only reached a so-called pachytene-like stage: First, the testis-specific histone variant H1t, a molecular marker for determining entry into mid-pachytene (Drabent et al., 1996), only faintly decorated the chromatin of those *Cdk2*$^{-/-}$ spermatocytes showing the highest levels of synapsis. Second, in *Cdk2*$^{-/-}$ spermatocytes we did not observe the typical redistribution of H3K9tri-m at chromocentres that encompasses the entry into pachytene in wild-type spermatocytes (Peters et al., 2001). Consequently, CDK2 is needed to complete progression throughout pachytene.

We have found that in the most advanced *Cdk2*$^{-/-}$ pachytene-like spermatocytes, synapsis was incomplete. Previously, several knockout mice have demonstrated defective synapsis, whose effects can be grouped into four main categories. The first category implies a complete lack of homologous synapsis, as occurs in knockout mice for the SC transverse filaments protein SYCP1 (de Vries et al., 2005) and also for the meiotic protein TEX15 (Yang et al., 2008a). The second category involves a correct initiation of synapsis between homologues, but a failure to fully achieve synapsis, as happens in knockout mice for the synaptonemal complex AE/LE proteins SYCP3 (Yuan et al., 2000) and SYCP2 (Yang et al., 2006), and for the CE proteins SYCE2 (Bolcun-Filas et al., 2007) and TEX12 (Hamer et al., 2008). The third category implies the absence of homologous synapsis for only some chromosomes, as occurs in mutants for the transition nodule protein TEX11 (Yang et al., 2008b). Finally, the fourth category involves the occurrence of non-homologous synapsis. Our results demonstrate that CDK2 knockout male mice belong to this fourth category. In this sense, in *Cdk2*$^{-/-}$ pachytene-like spermatocytes there is a high number of partner

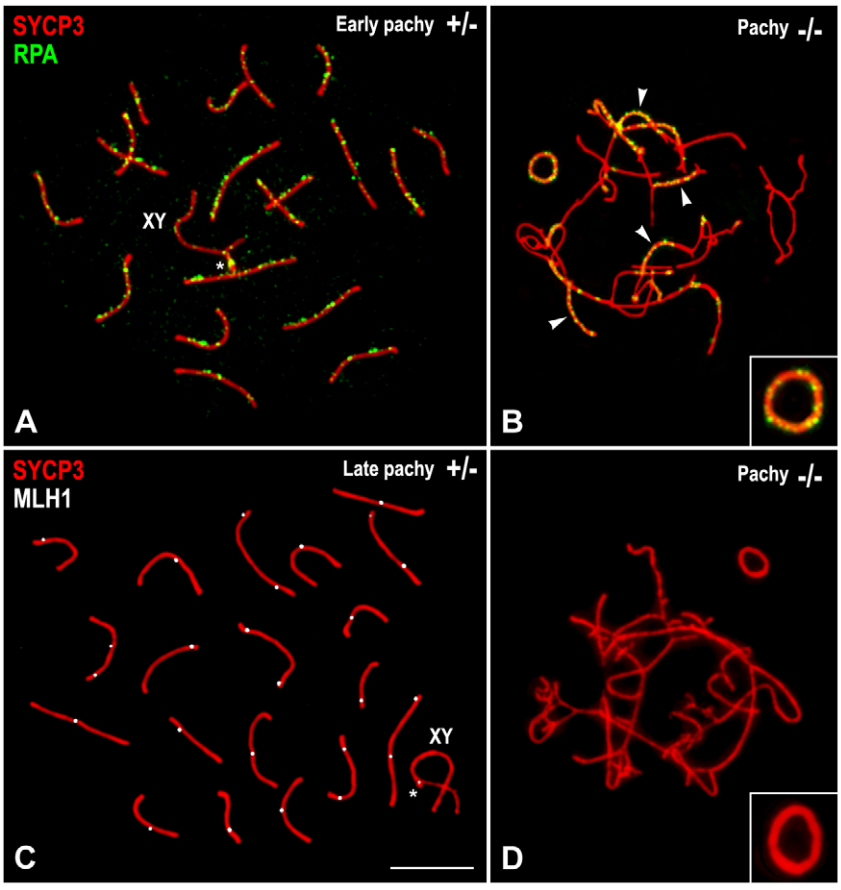

Fig. 7. *Cdk2*$^{-/-}$ spermatocytes do not repair DSBs. Double-immunolabelling of SYCP3 (red) with either RPA (green in A,B) or MLH1 (white in C,D) in *Cdk2*$^{+/-}$ pachytene (A,C) and *Cdk2*$^{-/-}$ pachytene-like (B,D) spread spermatocytes. (A) In *Cdk2*$^{+/-}$ pachytene spermatocytes, RPA foci are mainly distributed over the synapsed autosomal LEs, but also at the synapsed and asynapsed regions of the sex chromosome AEs. (B) In *Cdk2*$^{-/-}$ pachytene-like spermatocytes RPA foci are preferentially concentrated at synapsed regions (arrowheads), as well as in the ring chromosomes. (C) In *Cdk2*$^{+/-}$ pachytene spermatocytes MLH1 foci appear at recombination nodules in all bivalents, whereas these foci are not detected in *Cdk2*$^{-/-}$ pachytene-like spermatocytes (D). Inserts in B and D correspond to the ring chromosomes observed in the corresponding figure. The sex bivalent (XY) and the PAR (asterisk) are indicated. Scale bar: 10 μm.

switches of the LEs, as well as the presence of centromeres and telomeres along fully synapsed regions, indicating an extensive non-homologous synapsis. The formation of an SC between non-homologous chromosomes has been previously shown for a few other knockout mice for the proteins SPO11 (Baudat et al., 2000; Romanienko and Camerini-Otero, 2000), HOP2 (Petukhova et al., 2003), FKBP6 (Crackower et al., 2003) and the histone methyltransferases SUV39H (Peters et al., 2001). Consequently, we suggest that, like these other proteins, CDK2 is essential in certain crucial steps for homology search and for synapsis progression, although the specific processes and their underlying molecular mechanisms are still far from our understanding. However, as discussed below, a potential role of CDK2 at telomeres could also explain, at least in part, this phenotype.

CDK2 is implicated in telomere dynamics during prophase I

Meiotic chromosomes must attach to the NE by their telomeres during prophase I to provide chromosomal motility in order to facilitate the recognition between homologues, and their subsequent recombination and synapsis (for a review, see Scherthan, 2007). Our data on spread *Cdk2*$^{-/-}$ pachytene-like spermatocytes demonstrate that, unlike telomeres in wild-type or heterozygous pachytene spermatocytes, some telomeres are found along synapsed regions involved in heterologous synapsis. It has been reported that, in the mouse, CDK2 is present at telomeres during all stages of prophase I, both in spermatocytes and oocytes (supplementary material Fig. S3) (Ashley et al., 2001); however, nothing is known of the possible roles of CDK2 at telomeres. The authors proposed that since CDK2 also localised at recombination nodules, this dual localisation might be due to the structural similarities between telomeric DNA t-loops (Griffith et al., 1999) (for a review, see Gilson and Géli, 2007) and the Holliday junction intermediates formed during early recombination (for a review, see Liu and West, 2004). Moreover, our results suggest that one of the possible roles of CDK2 at telomeres is to allow their proper attachment to the NE. If some telomeres do not attach to the NE in leptotene and early zygotene, the correct 'bouquet' distribution of telomeres would not take place. This circumstance could prevent an accurate homology search, leading to extensive non-homologous pairing. Additionally, the appearance of ring chromosome structures in the absence of CDK2, with SYCP1 along their length, and two closely associated centromeres and telomeres, might indicate the possible circularisation of a SC through association of their proximal and distal telomeres. Consequently, CDK2 could also be involved in telomere capping by the establishment and/or stabilisation of t-loops. In the absence of CDK2, telomeres could fuse and give rise to ring chromosomes or even chromosome end-to-end fusions, such as those we have observed. Therefore, our results reveal that CDK2 has an essential role in telomere maintenance and homeostasis during mammalian meiosis; its absence prevents the proper telomeric interaction of chromosomes with the NE and promotes aberrant telomere associations.

CDK2 is required for sex-body formation

We have found that in *Cdk2*$^{-/-}$ spermatocytes a canonical sex body is not detected by either DAPI or γ-H2AX (Fernández-Capetillo et al., 2003) staining. Since unsynapsed sex chromosome AEs were not detected, we reason that, unexpectedly, the sex AEs must be involved in non-homologous synapsis with autosomes. Consequently, the pairing deficiencies in the absence of CDK2 affect both the autosomes and sex chromosomes. Sex bodies are not developed in other knockout mice, such as those lacking the SC transverse filament protein SYCP1 (de Vries et al., 2005) or the SC central element protein SYCE2 (Bolcun-Filas et al., 2007). However, the original cause of the absence of sex-body establishment in these mutants is different from that occurring in *Cdk2*$^{-/-}$ mutants because, unlike *Cdk2*$^{-/-}$ spermatocytes, in these mutants synapsis is inhibited.

It has been reported that BRCA1 and ATR appear at asynapsed sex chromosome AEs and sex chromatin during pachytene (Turner et al., 2004). These authors have suggested that BRCA1 recruits the kinase ATR to sex chromosomes and that ATR phosphorylates the histone H2AX, which in turn triggers the formation of the sex body and ensuing transcriptional silencing of sex chromosomes. Our results show that, in *Cdk2*$^{-/-}$ pachytene-like spermatocytes, BRCA1 is not detected on AEs/LEs and that ATR, as in *Brca1*$^{-/-}$ pachytene spermatocytes (Turner et al., 2004), is present at both synapsed and unsynapsed regions. We suggest that since BRCA1 is not loaded on sex chromosomes, ATR is not recruited to them and a sex body is not formed in the absence of CDK2. Interestingly, it is reported that CDK2 is able to phosphorylate BRCA1 (Ruffner et al., 1999; Hayami et al., 2005). Thus, it is tempting to suggest that BRCA1 is not properly phosphorylated in *Cdk2*$^{-/-}$ spermatocytes and that this is, at least in part, what prevents it from being loaded on sex chromosomes; consequently, the formation of a sex body through ATR recruitment and H2AX phosphorylation does not take place. This hypothesis requires further investigation, but is supported by the fact that mice lacking functional BRCA1 present abnormalities in sex-body formation (Xu et al., 2003). An alternative, but not mutually exclusive possibility, is that since the telomere dynamics is altered in *Cdk2*$^{-/-}$ spermatocytes, sex chromosomes are not able to pair (as detected by fluorescent in situ hybridisation, FISH) and consequently a sex body is not formed.

CDK2 is involved in processing of DSBs

The presence of γ-H2AX domains in *Cdk2*$^{-/-}$ leptotene and zygotene spermatocytes demonstrates a correct initiation of meiotic recombination, regarding the initial formation of DSBs, as described in wild-type mice (Mahadevaiah et al., 2001). However, although γ-H2AX is mainly restricted to the sex body in wild-type pachytene spermatocytes, *Cdk2*$^{-/-}$ pachytene-like spermatocytes showed persisting γ-H2AX chromosomal domains protruding from both unsynapsed and synapsed LEs. This result indicates the accumulation of non-repaired DSBs in *Cdk2*$^{-/-}$ pachytene-like spermatocytes. To corroborate this hypothesis, we analysed the distribution of RAD51 and RPA in *Cdk2*$^{-/-}$ spermatocytes. RAD51 is a recombinase found at early nodules that is attached to the resected single-strand ends flanking a DSB (Hunter and Kleckner, 2001; Moens et al., 2007) and is involved in the homology search. RPA is a single-stranded DNA-binding protein that interacts with RAD51 during the strand-exchange reaction that is found at transition nodules (Sigurdsson et al., 2001; Moens et al., 2007). The presence of RAD51 and RPA foci along AEs/LEs in *Cdk2*$^{-/-}$ zygotene spermatocytes and their persistence in pachytene-like spermatocytes (mainly at the unsynapsed and synapsed regions, respectively) support the idea that the processing and repair of DSBs is initiated in the absence of CDK2, but not concluded. Moreover, the absence of MLH1 in *Cdk2*$^{-/-}$ pachytene-like spermatocytes further suggests that DSBs are not repaired in the mutant. Consequently, CDK2 is involved in the processing and repair of meiotic DSBs. This is consistent with previous data demonstrating that CDK2 plays a crucial role in normal DSB repair in somatic

cells (Aylon et al., 2004; Müller-Tidow et al., 2004; Deans et al., 2006).

CDK2 is located at recombination nodules in wild-type pachytene spermatocytes (supplementary material Fig. S3) (Ashley et al., 2001). However, although CDK2 is not cytologically detected at early and transition nodules during leptotene and zygotene, its direct participation in the early processing of DSBs cannot be excluded. As discussed above, CDK2 can phosphorylate BRCA1 (Ruffner et al., 1999; Hayami et al., 2005), which in mouse meiosis appears at early nodules colocalising with RAD51 (Keegan et al., 1996; Scully et al., 1997). In somatic cells, BRCA1 interacts with BRCA2 and regulates RAD51 function in response to DNA damage (Cousineau et al., 2005). Thus, we hypothesise that in *Cdk2*$^{-/-}$ spermatocytes BRCA1 may not be properly phosphorylated and that this may have an impact on RAD51 function and or localisation, which in turn leads to an arrest in the processing of DSBs. Moreover, it is known that RAD51 acts in concert with the HOP2-MND1 complex during mammalian meiotic recombination to promote proper homologous pairing (Petukhova et al., 2005; Pezza et al., 2007). In fact, *Hop2*$^{-/-}$ spermatocytes, like those lacking CDK2, undergo SC formation among non-homologous chromosomes and arrest at a pachytene-like stage with unrepaired DSBs (Petukhova et al., 2003). Thus, another mechanism by which the absence of CDK2 may promote non-homologous pairing is by inhibiting RAD51 function during DSB processing.

In summary, we conclude that CDK2 is required during prophase I of male meiosis for the correct processing of programmed DSBs and further recombination, and also for the accuracy of homologous chromosome synapsis and telomere function. The identity of the protein or proteins acting as partners of CDK2 in these different processes is not known. During mouse meiosis, cyclin A1, a putative catalytic partner of CDK2 appears at centromeres and, unlike *Cdk2*$^{-/-}$ spermatocytes, those of cyclin A1-deficient mice arrest at late diplotene (Nickerson et al., 2007). Thus, we suggest that another type of CDK2-binding cyclin (such as cyclin E or cyclin B3) or a CDK2 non-cyclin activator (such as one of the RINGO protein family members) might act as the catalytic partner of CDK2 during early meiotic prophase. Interestingly, a specific time-frame for CDK2 activation and/or expression seems to be crucial for the function of CDK2 during meiosis. Genetic replacement of one copy of CDK1 by CDK2, in a *Cdk2*$^{-/-}$ background does not rescue the meiotic phenotype of *Cdk2*$^{-/-}$ mice, even when the cellular localisation properties and levels of the CDK2 protein expressed from the Cdk1 locus seem to be similar to those of the endogenous protein (Satyanarayana et al., 2008). Further studies need to be performed to identify the meiotic partner(s) of CDK2 and to understand the function of CDK2 in meiosis at the molecular level.

Materials and Methods

Squashing of seminiferous tubules and spreading of spermatocytes

Adult male C57BL/6 mice and adult *Cdk2*$^{+/-}$ and *Cdk2*$^{-/-}$ mice (Ortega et al., 2003) were used for this study. Mice were kept under SPF barrier conditions at the CNIO animal facility. Testes were removed, detunicated, and the seminiferous tubules processed for either squashing or spreading. For squashing, we followed the technique previously described (Page et al., 1998; Parra et al., 2002). For spreading of spermatocytes, we followed the drying-down technique previously described by Peters et al. (Peters et al., 1997).

Immunofluorescence microscopy

After fixation, the spread or squashed preparations were rinsed three times for 5 minutes in PBS, and incubated overnight at 4°C with the corresponding primary antibodies diluted in PBS. To detect SYCP3 we employed either a mouse monoclonal antibody (ab-12452; Abcam, Cambridge, MA) or the rabbit polyclonal serum A1 (a gift from Christa Heyting; Wageningen University, Wageningen, The Netherlands) at a 1:500 dilution. The rabbit polyclonal serum A2 was used to recognise the SYCP1 protein (a gift from Christa Heyting) at a 1:200 dilution. INCENP was detected with the rabbit polyclonal serum 1186 (a gift from William Earnshaw, University of Edinburgh, Edinburgh, UK) at a 1:100 dilution. SYCP2 was detected with the rabbit polyclonal serum 493 (a gift from Christa Heyting) at a 1:100 dilution. The cohesin subunit RAD21 was detected with the rabbit polyclonal serum K854 (Prieto et al., 2002) at a 1:50 dilution. The histone H1t was detected with a guinea-pig polyclonal antibody (a gift from Mary Ann Handel, The Jackson Laboratory, Bar Harbor, ME) at a 1:100 dilution. H3K9tri-m was revealed with a rabbit polyclonal serum (ab-8898; Abcam) at a 1:100 dilution. ATR was detected with a goat polyclonal serum (sc-1887; Santa Cruz Biotechnology) at a 1:100 dilution. A goat polyclonal serum generated against mouse BRCA1 (sc-1553; Santa Cruz Biotechnology) was used at a 1:10 dilution. Kinetochores were revealed with a human anti-centromere antibody (ACA) (15-235; Antibodies Incorporated, Davis, CA) at a 1:100 dilution. To detect TRF1 we used a rabbit polyclonal serum (TRF 12-S; Alpha Diagnostic International, San Antonio, TX), raised against mouse TRF1, at a 1:50 dilution. To detect γ-H2AX we used a monoclonal mouse antibody (05-636; Upstate, Charlottesville, VA) at a 1:1,000 dilution. A rabbit polyclonal anti-RAD51 antibody (Ab-1, PC130; Oncogene Research Products, Cambridge, MA), generated against recombinant HsRad51 protein, was used at a 1:50 dilution. RPA was detected with a rabbit polyclonal serum (a gift from Peter Moens, York University, Toronto, Canada) at a 1:100 dilution. A mouse monoclonal anti-MLH1 antibody (551091; Pharmingen, San Diego, CA) was used at a 1:10 dilution. Following three washes in PBS, the slides were incubated for 30 minutes at room temperature with secondary antibodies diluted in PBS. The appropriated combinations of the following secondary antibodies were employed for simultaneous double-immunolabelling: a fluorescein isothiocyanate (FITC)-conjugated goat anti-mouse IgG (Jackson, West Grove, PA) at a 1:150 dilution, a Texas-red-conjugated donkey anti-mouse ML IgG (Jackson) at a 1:150 dilution, a Texas-red-conjugated goat anti-human IgG (Jackson) at a 1:150 dilution, a FITC-conjugated donkey anti-rabbit ML IgG (Jackson) at a 1:150 dilution, a Texas-red-conjugated donkey anti-rabbit ML IgG (Jackson) at a 1:150 dilution, a Texas-red-conjugated donkey anti-goat ML IgG (Jackson) at a 1:40 dilution, and a FITC-conjugated donkey anti-guinea-pig ML IgG (Jackson) at a 1:150 dilution. The slides were subsequently rinsed in PBS, and counterstained for 3 minutes with 5 μg/ml DAPI. After a final rinse in PBS, the slides were mounted in Vectashield (Vector Laboratories, Burlingame, CA) and sealed with nail varnish. In double-immunolabelling experiments, primary antibodies were incubated simultaneously. The triple immunolabelling of SYCP3, γ-H2AX and RAD51, in which two primary antibodies were generated in the same host species (SYCP3 and γ-H2AX), was carried out as described by Viera et al. (Viera et al., 2003).

Observations were performed using an Olympus BX61 microscope equipped with a motorised Z axis and epifluorescence optics. Image stacks were captured with an Olympus DP70 digital camera controlled by analySIS software (Soft Imaging System), and analysed and processed for making figures or movies using the public domain ImageJ software (NIH, Bethesda, MD; http://rsb.info.nih.gov/ij). Final images were processed with Adobe Photoshop 7.0 software.

Immunofluorescence and FISH

The XY chromosome FISH was performed after immunostaining spermatocyte spreads with SYCP3 as described above. Slides were washed for 2 minutes in distilled water, left to dry at room temperature and denatured for 5 minutes at 70°C in 70% formamide in 2×SSC (pH 7.5). After washing for 1 minute in distilled water, 100 μl of 1M sodium thiocyanate was applied and the slides incubated for 3 hours at 65°C. Subsequently, slides were again denatured and dehydrated in ice-cold 70%, 80% and 100% ethanol series for 1 minute. The appropriate amount of ready-to-use hybridisation solution containing the Cy3-conjugated chromosome painting X probe (1200-XMCy3-01; Cambio, Cambridge, UK) and FITC-conjugated chromosome painting Y probe (1189-YMF-01; Cambio) was prepared, denatured for 10 minutes at 70°C, and incubated for 30-60 minutes at 37°C. The hybridisation solution was added to dried slides, a coverslip applied and sealed, and preparations hybridised for 72 hours in a moist chamber at 37°C. After a final rinse in 0.05×SSC at 45°C, slides were counterstained with DAPI and mounted.

We wish to express our sincere thanks to Christa Heyting, Bill Earnshaw, Peter Moens and Mary Ann Handel for providing antibodies. We also thank Lucía Aguilar, Miriam García and Isabel Blanco, from the Animal Facility at the CNIO, for their help with mouse maintenance. This work was supported by Ministerio de Educación y Ciencia grants BFU2005-05668-C03 (to S.O. and J.A.S.), BFU2006-06655 (to J.S.R.), and BFU2006-04406 (to J.L.B.), and Comunidad de Madrid grants GR/SAL/0206/2004 and P-BIO-0189-2006 (to J.L.B.).

References

Ashley, T., Walpita, D. and de Rooij, D. G. (2001). Localization of two mammalian cyclin dependent kinases during mammalian meiosis. *J. Cell Sci.* **114**, 685-693.

Aylon, Y., Liefshitz, B. and Kupiec, M. (2004). The CDK regulates repair of double-strand breaks by homologous recombination during the cell cycle. *EMBO J.* **23**, 4868-4875.

Baker, S. M., Plug, A. W., Prolla, T. A., Bronner, C. E., Harris, A. C., Yao, X., Christie, D. M., Monell, C., Arnheim, N., Bradley, A. et al. (1996). Involvement of mouse Mlh1 in DNA mismatch repair and meiotic crossing over. *Nat. Genet.* **13**, 336-342.

Baudat, F., Manova, K., Yuen, J. P., Jasin, M. and Keeney, S. (2000). Chromosome synapsis defects and sexually dimorphic meiotic progression in mice lacking Spo11. *Mol. Cell* **6**, 989-998.

Berthet, C., Aleem, E., Coppola, V., Tessarollo, L. and Kaldis, P. (2003). Cdk2 knockout mice are viable. *Curr. Biol.* **13**, 1775-1785.

Bolcun-Filas, E., Costa, Y., Speed, R., Taggart, M., Benavente, R., De Rooij, D. and Cooke, H. J. (2007). SYCE2 is required for synaptonemal complex assembly, double strand break repair, and homologous recombination. *J. Cell Biol.* **176**, 741-747.

Cousineau, I., Abaji, C. and Belmaaza, A. (2005). BRCA1 regulates RAD51 function in response to DNA damage and suppresses spontaneous sister chromatid replication slippage: implications for sister chromatid cohesion, genome stability, and carcinogenesis. *Cancer Res.* **65**, 11384-11391.

Crackower, M. A., Kolas, N. K., Noguchi, J., Sarao, R., Kikuchi, K., Kaneko, H., Kobayashi, E., Kawai, Y., Kozieradzki, I., Landers, R. et al. (2003). Essential role of Fkbp6 in male fertility and homologous chromosome pairing in meiosis. *Science* **300**, 1291-1295.

Deans, A. J., Khanna, K. K., McNees, C. J., Mercurio, C., Heierhorst, J. and McArthur, G. A. (2006). Cyclin-dependent kinase 2 functions in normal DNA repair and is a therapeutic target in BRCA1-deficient cancers. *Cancer Res.* **66**, 8219-8226.

de Vries, F. A., de Boer, E., van den Bosch, M., Baarends, W. M., Ooms, M., Yuan, L., Liu, J. G., van Zeeland, A. A., Heyting, C. and Pastink, A. (2005). Mouse Sycp1 functions in synaptonemal complex assembly, meiotic recombination, and XY body formation. *Genes Dev.* **19**, 1376-1389.

Drabent, B., Bode, C., Bramlage, B. and Doenecke, D. (1996). Expression of the mouse testicular histone gene H1t during spermatogenesis. *Histochem. Cell Biol.* **106**, 247-251.

Fernández-Capetillo, O., Mahadevaiah, S. K., Celeste, A., Romanienko, P. J., Camerini-Otero, R. D., Bonner, W. M., Manova, K., Burgoyne, P. and Nussenzweig, A. (2003). H2AX is required for chromatin remodeling and inactivation of sex chromosomes in male mouse meiosis. *Dev. Cell* **4**, 497-508.

Gilson, E. and Géli, V. (2007). How telomeres are replicated. *Nat. Rev. Mol. Cell. Biol.* **8**, 825-838.

Griffith, J. D., Comeau, L., Rosenfield, S., Stansel, R. M., Bianchi, A., Moss, H. and de Lange, T. (1999). Mammalian telomeres end in a large duplex loop. *Cell* **97**, 503-514.

Hamer, G., Wang, H., Bolcun-Filas, E., Cooke, H. J., Benavente, R. and Höög, C. (2008). Progression of meiotic recombination requires structural maturation of the central element of the synaptonemal complex. *J. Cell Sci.* **121**, 2445-2451.

Hayami, R., Sato, K., Wu, W., Nishikawa, T., Hiroi, J., Ohtani-Kaneko, R., Fukuda, M. and Ohta, T. (2005). Down-regulation of BRCA1-1 ubiquitin ligase by CDK2. *Cancer Res.* **65**, 6-10.

Hochegger, H., Takeda, S. and Hunt, T. (2008). Cyclin-dependent kinases and cell-cycle transitions: does one fit all? *Nat. Rev. Mol. Cell. Biol.* **9**, 910-916.

Hunter, N. and Kleckner, N. (2001). The single-end invasion: an asymmetric intermediate at the double-strand break to double-holliday junction transition of meiotic recombination. *Cell* **106**, 59-70.

Keegan, K. S., Holtzman, D. A., Plug, A. W., Christenson, E. R., Brainerd, E. E., Flaggs, G., Bentley, N. J., Taylor, E. M., Meyn, M. S., Moss, S. B. et al. (1996). The Atr and Atm protein kinases associate with different sites along meiotically pairing chromosomes. *Genes Dev.* **10**, 2423-2437.

Lachner, M., O'Carroll, D., Rea, S., Mechtler, K. and Jenuwein, T. (2001). Methylation of histone H3 lysine 9 creates a binding site for HP1 proteins. *Nature* **410**, 116-120.

Liu, Y. and West, S. C. (2004). Happy Hollidays: 40th anniversary of the Holliday junction. *Nat. Rev. Mol. Cell. Biol.* **5**, 937-944.

Mahadevaiah, S. K., Turner, J. M., Baudat, F., Rogakou, E. P., de Boer, P., Blanco-Rodriguez, J., Jasin, M., Keeney, S., Bonner, W. M. and Burgoyne, P. S. (2001). Recombinational DNA double-strand breaks in mice precede synapsis. *Nat. Genet.* **27**, 271-276.

Malumbres, M. (2005). Revisiting the "Cdk-centric" view of the mammalian cell cycle. *Cell Cycle* **4**, 206-210.

Malumbres, M. and Barbacid, M. (2005). Mammalian cyclin-dependent kinases. *Trends Biochem. Sci.* **30**, 630-641.

Moens, P. B., Kolas, N. K., Tarsounas, M., Marcon, E., Cohen, P. E. and Spyropoulos, B. (2002). The time course and chromosomal localization of recombination-related proteins at meiosis in the mouse are compatible with models that can resolve the early DNA-DNA interactions without reciprocal recombination. *J. Cell Sci.* **115**, 1611-1622.

Moens, P. B., Marcon, E., Shore, J. S., Kochakpour, N. and Spyropoulos, B. (2007). Initiation and resolution of interhomolog connections: crossover and non-crossover sites along mouse synaptonemal complexes. *J. Cell Sci.* **120**, 1017-1027.

Müller-Tidow, C., Ji, P., Diederichs, S., Potratz, J., Bäumer, N., Köhler, G., Cauvet, T., Choudary, C., van der Meer, T., Chan, W. Y. et al. (2004). The cyclin A1-CDK2 complex regulates DNA double-strand break repair. *Mol. Cell. Biol.* **24**, 8917-8928.

Nickerson, H. D., Joshi, A. and Wolgemuth, D. J. (2007). Cyclin A1-deficient mice lack histone H3 serine 10 phosphorylation and exhibit altered aurora B dynamics in late prophase of male meiosis. *Dev. Biol.* **306**, 725-735.

Ortega, S., Prieto, I., Odajima, J., Martín, A., Dubus, P., Sotillo, R., Barbero, J. L., Malumbres, M. and Barbacid, M. (2003). Cyclin-dependent kinase 2 is essential for meiosis but not for mitotic cell division in mice. *Nat. Genet.* **35**, 25-31.

Page, J., Suja, J. A., Santos, J. L. and Rufas, J. S. (1998). Squash procedure for protein immunolocalisation in meiotic cells. *Chromosome Res.* **6**, 639-642.

Parra, M. T., Page, J., Yen, T. J., He, D., Valdeolmillos, A., Rufas, J. S. and Suja, J. A. (2002). Expression and behaviour of CENP-E at kinetochores during mouse spermatogenesis. *Chromosoma* **111**, 53-61.

Parra, M. T., Viera, A., Gómez, R., Page, J., Carmena, M., Earnshaw, W. C., Rufas, J. S. and Suja, J. A. (2003). Dynamic relocalization of the chromosomal passenger complex proteins inner centromere protein (INCENP) and aurora-B kinase during male mouse meiosis. *J. Cell Sci.* **116**, 961-974.

Parra, M. T., Viera, A., Gómez, R., Page, J., Benavente, R., Santos, J. L., Rufas, J. S. and Suja, J. A. (2004). Involvement of the cohesin Rad21 and SCP3 in monopolar attachment of sister kinetochores during mouse meiosis I. *J. Cell Sci.* **117**, 1221-1234.

Peters, A. H., Plug, A. W., van Vugt, M. J. and de Boer, P. (1997). A drying-down technique for the spreading of mammalian meiocytes from the male and female germline. *Chromosome Res.* **5**, 66-68.

Peters, A. H., O'Carroll, D., Scherthan, H., Mechtler, K., Sauer, S., Schofer, C., Weipoltshammer, K., Pagani, M., Lachner, M., Kohlmaier, A. et al. (2001). Loss of the Suv39h histone methyltransferases impairs mammalian heterochromatin and genome stability. *Cell* **107**, 323-337.

Petukhova, G. V., Romanienko, P. J. and Camerini-Otero, R. D. (2003). The Hop2 protein has a direct role in promoting interhomolog interactions during mouse meiosis. *Dev. Cell* **5**, 927-936.

Petukhova, G. V., Pezza, R. J., Vanevski, F., Ploquin, M., Masson, J. Y. and Camerini-Otero, R. D. (2005). The Hop2 and Mnd1 proteins act in concert with Rad51 and Dmc1 in meiotic recombination. *Nat. Struct. Mol. Biol.* **12**, 449-453.

Pezza, R. J., Voloshin, O. N., Vanevski, F. and Camerini-Otero, R. D. (2007). Hop2/Mnd1 acts on two critical steps in Dmc1-promoted homologous pairing. *Genes Dev.* **21**, 1758-1766.

Prieto, I., Pezzi, N., Buesa, J. M., Kremer, L., Barthelemy, I., Carreiro, C., Roncal, F., Martínez, A., Gómez, L., Fernández, R. et al. (2002). STAG2 and Rad21 mammalian mitotic cohesins are implicated in meiosis. *EMBO Rep.* **3**, 543-550.

Romanienko, P. J. and Camerini-Otero, R. D. (2000). The mouse Spo11 gene is required for meiotic chromosome synapsis. *Mol. Cell* **6**, 975-987.

Ruffner, H., Jiang, W., Craig, A. G., Hunter, T. and Verma, I. M. (1999). BRCA1 is phosphorylated at serine 1497 in vivo at a cyclin-dependent kinase 2 phosphorylation site. *Mol. Cell. Biol.* **19**, 4843-4854.

Santamaria, D. and Ortega, S. (2006). Cyclins and CDKS in development and cancer: lessons from genetically modified mice. *Front. Biosci.* **11**, 1164-1188.

Satyanarayana, A, Berthet, C., Lopez-Molina, J., Coppola, V., Tessarollo, L. and Kaldis, P. (2008). Genetic substitution of Cdk1 by Cdk2 leads to embryonic lethality and loss of meiotic function of Cdk2. *Development* **135**, 3389-3400.

Scherthan, H. (2007). Telomere attachment and clustering during meiosis. *Cell. Mol. Life Sci.* **64**, 117-124.

Scherthan, H., Jerratsch, M., Li, B., Smith, S., Hultén, M., Lock, T. and de Lange, T. (2000). Mammalian meiotic telomeres: protein composition and redistribution in relation to nuclear pores. *Mol. Biol. Cell* **11**, 4189-4203.

Scully, R., Chen, J., Plug, A., Xiao, Y., Weaver, D., Feunteun, J., Ashley, T. and Livingston, D. M. (1997). Association of BRCA1 with Rad51 in mitotic and meiotic cells. *Cell* **88**, 265-275.

Sigurdsson, S., Trujillo, K., Song, B., Stratton, S. and Sung, P. (2001). Basis for avid homologous DNA strand exchange by human Rad51 and RPA. *J. Biol. Chem.* **276**, 8798-8806.

Suja, J. A. and Barbero, J. L. (2009). Cohesin complexes and sister chromatid cohesion in mammalian meiosis. *Genome Dyn.* **5**, 94-116.

Svetlanov, A. and Cohen, P. E. (2004). Mismatch repair proteins, meiosis, and mice: understanding the complexities of mammalian meiosis. *Exp. Cell Res.* **296**, 71-79.

Tetsu, O. and McCormick, F. (2003). Proliferation of cancer cells despite CDK2 inhibition. *Cancer Cell* **3**, 233-245.

Turner, J. M., Aprelikova, O., Xu, X., Wang, R., Kim, S., Chandramouli, G. V., Barrett, J. C., Burgoyne, P. S. and Deng, C. X. (2004). BRCA1, histone H2AX phosphorylation, and male meiotic sex chromosome inactivation. *Curr. Biol.* **14**, 2135-2142.

Viera, A., Parra, M. T., Page, J., Santos, J. L., Rufas, J. S. and Suja, J. A. (2003). Dynamic relocation of telomere complexes in mouse meiotic chromosomes. *Chromosome Res.* **11**, 797-807.

Xu, X., Aprelikova, O., Moens, P., Deng, C. X. and Furth, P. A. (2003). Impaired meiotic DNA-damage repair and lack of crossing-over during spermatogenesis in BRCA1 full-length isoform deficient mice. *Development* **130**, 2001-2012.

Yang, F., De La, Fuente, R., Leu, N. A., Baumann, C., McLaughlin, K. J. and Wang, P. J. (2006). Mouse SYCP2 is required for synaptonemal complex assembly and chromosomal synapsis during male meiosis. *J. Cell Biol.* **173**, 497-507.

Yang, F., Eckardt, S., Leu, N. A., McLaughlin, K. J. and Wang, P. J. (2008a). Mouse TEX15 is essential for DNA double-strand break repair and chromosomal synapsis during male meiosis. *J. Cell Biol.* **180**, 673-679.

Yang, F., Gell, K., van der Heijden, G. W., Eckardt, S., Leu, N. A., Page, D. C., Benavente, R., Her, C., Höög, C., McLaughlin, K. J. et al. (2008b). Meiotic failure in male mice lacking an X-linked factor. *Genes Dev.* **22**, 682-691.

Yuan, L., Liu, J. G., Zhao, J., Brundell, E., Daneholt, B. and Höög, C. (2000). The murine SCP3 gene is required for synaptonemal complex assembly, chromosome synapsis, and male fertility. *Mol. Cell* **5**, 73-83.